Irreversible magnetic response of the simplest three-dimensional Josephson-junction network

R. De Luca and S. Pace
Istituto Nazionale di Fisica Nucleare and Dipartimento di Fisica, Università degli Studi di Salerno, I-84081 Baronissi, Salerno, Italy

C. Auletta and G. Raiconi
Dipartimento di Informatica, Università degli Studi di Salerno, I-84081 Baronissi, Salerno, Italy
(Received 22 March 1995)

We describe the stationary magnetic states of the simplest three-dimensional (3D) Josephson-junction network, namely, a tetrahedron containing a junction on each side. In this system the Josephson junctions are coupled through inductances and the externally applied magnetic field **H** is directed along an arbitrary direction in space. We give a complete analytic treatment of the problem taking into account fluxoid quantization for each loop in the network. We also determine the lower threshold field H_{gc1} for irreversible flux penetration for the tetrahedral network for two orientations of the field **H**, one perpendicular and one parallel to the base of the tetrahedron.

I. INTRODUCTION

Networks of Josephson junctions (JJ's) have been extensively used in the study of the electrodynamical properties of high-T_c granular superconductors.[1–4] Indeed, granular superconductors can be seen as a 3D collection of superconducting grains weakly coupled to their next neighbors.

In general, it is sufficient to study two-dimensional JJ arrays[2–4] in order to predict the magnetic response of granular superconductors. This dimensional reduction is in most cases due to the particular symmetry of the problem under examination, as, for example, a magnetic field applied in the axial direction of an infinite cylinder. Among the magnetic properties of 2D JJ networks we may cite the presence of a lower threshold field for irreversible flux penetration H_{gc1}.[5] In fact, after zero-field cooling (ZFC), for very low values of the external field (applied in the direction perpendicular to the plane of the network) and for a relatively strong coupling among the grains, 2D systems do not allow irreversible flux penetration until the first threshold field H_{gc1} is reached. For $H > H_{gc1}$, flux quanta penetrate the network irreversibly in much the same way as Abrikosov vortices nucleate in hard type-II superconductors. Indeed, in this low-field irreversible regime, a critical state picture, in which the critical current is identified with the maximum Josephson current of the junctions, can be detected by means of numerical analyses.[3,6,7] The particular critical state model to be adopted in this case has been suggested, by means of experimental and analytical studies on ceramic $YBa_2Cu_3O_{7-x}$, by Ginzburg *et al.*;[8] they found the following local field dependence of the critical current density J_c:

$$\frac{J_c(h,T)}{J_{c0}(T)} = \frac{H_0^2(T)}{H_0^2(T)+h^2}\ , \tag{1}$$

where $h = h(r)$ is the local magnetic field, J_{c0} is the zero-field value of the critical current density, and H_0 is a temperature-dependent measure of the width of the bell-shaped curve of Eq. (1). This critical state picture is compatible with the JJ array description of the copper-oxide superconducting systems. Indeed, it can be shown[9] that the low-field Taylor series expansion of Eq. (1) has a quadratic leading order term as in the case of the charac-

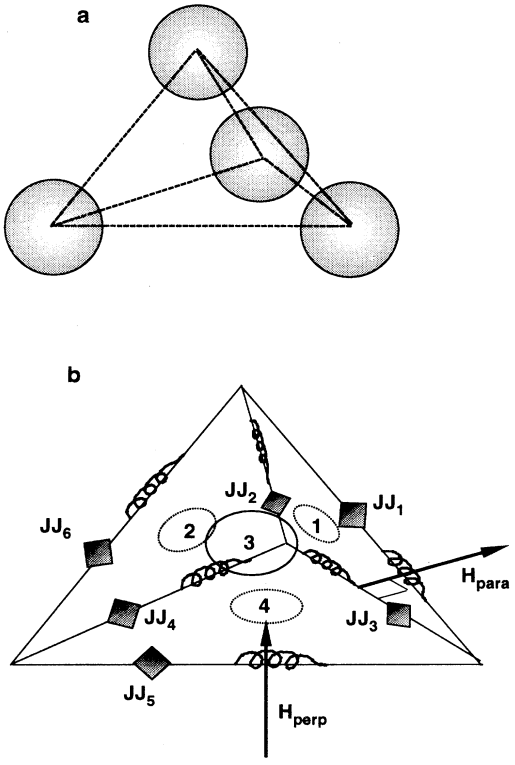

FIG. 1. (a) The simplest three-dimensional granular system: four grains in a tetrahedral arrangement. (b) Equivalent network of Josephson junctions and inductances for the study of the electrodynamic properties of the physical system shown in (a). The diamonds are Josephson junctions (JJ's) and the tetrahedron faces are numbered from 1 to 4.

teristic Fraunhofer pattern giving the field dependence of the maximum Josephson current of a single small rectangular or circular junction.[10,11] Therefore, if one is able to specify the temperature dependence of H_0 and of J_{c0}, one solves the problem of the low-field magnetic response of 2D JJ arrays. Recently, an effective critical current density function for a 2D network has been given by Constabile *et al.*[12] on the basis of numerical studies performed by Filatrella *et al.*[13] The temperature dependence of H_0 has been derived from the knowledge of the Fraunhofer pattern of a single small Josephson junction by De Luca.[9]

Very recently, the dynamics of tetrahedral Josephson-junction arrays has been studied by Yukon and Lin.[14] However, the stationary magnetic response of 3D JJ networks has not been analyzed in detail yet. In the present work, we thus consider the simplest 3D granular system: four identical grains in a tetrahedral arrangement [Fig. 1(a)]. The corresponding model network consists of a system of six JJ's, each lying on the side of a tetrahedron and each coupled to its next-neighboring JJ through inductances [Fig. 1(b)]. This system might be considered as a unit cell of a circuital model of a large cluster of grains coupled by small Josephson junctions.

Here we present a numerical study of the magnetic response of the four-grain system for arbitrary field orientations. In Sec. II we derive the dynamic equations describing the time evolution of the flux and current distributions. In Sec. III, by numerically integrating the system of differential equations found in the preceding section, we determine the stationary states after ZFC. In Sec. IV, the dependence of the lower threshold field value H_{gc1} on the effective coupling parameter between the junctions is derived for these systems. Conclusions are drawn in the last section.

II. THE EQUATIONS

In the system represented in Fig. 1(b) we take the effective intergranular area of a single tetrahedral face to be S_0. In this way, to each face of the tetrahedron can be associated an area vector $\mathbf{S}_i = S_0 \mathbf{n}_i$, $\mathbf{n}_i$ being the outward unit vector perpendicular to the ith face of the tetrahedron, with $i = 1, \ldots, 4$. The physical grains are taken to be perfectly diamagnetic extended spheres; as a consequence, the macroscopic superconducting phase of each sphere may vary with position. Each pair of grains is separated by a JJ, whose gauge-invariant phase difference, calculated at the grain interfaces, is denoted by φ_k, with k ranging from 1 to 6. By taking into account the self- and mutual inductance coefficients M_{ij} between the elementary current loops, the current-flux equations are

$$\Phi_i = \sum_{j=1}^{4} M_{ij} I_j + \mu_0 \mathbf{H} \cdot \mathbf{S}_i, \quad i = 1,4 , \tag{2}$$

where the quantity Φ_i is the flux linked to the ith face and I_i is the corresponding loop current, taken as positive if circulating in the counterclockwise sense, as seen from an observation point outside the tetrahedron.

Fluxoid quantization must hold for any closed loop interrupted by an arbitrary number of JJ's. Therefore, referring to Fig. 1(b), we get the following flux-phase relations:

$$\begin{aligned}
&-(\varphi_1+\varphi_2+\varphi_3)+\frac{2\pi\Phi_1}{\Phi_0}=2\pi N_1 , \\
&-\varphi_4-\varphi_6+\varphi_2+\frac{2\pi\Phi_2}{\Phi_0}=2\pi N_2 , \\
&-\varphi_5+\varphi_1+\varphi_6+\frac{2\pi\Phi_3}{\Phi_0}=2\pi N_3 , \\
&\varphi_3+\varphi_4+\varphi_5+\frac{2\pi\Phi_4}{\Phi_0}=2\pi N_4 ,
\end{aligned} \tag{3}$$

where N_1, N_2, N_3, and N_4 are integers. The right-hand side of the above equations would be null if we assumed zero-field cooling initial conditions. Neglecting capacitive effects, we can write the dynamic equations for the gauge-invariant phase differences φ_i by means of the resistively shunted junction (RSJ) model:[10]

$$\begin{aligned}
&\left[\frac{\Phi_0}{2\pi R_n}\right]\frac{d\varphi_1}{dt}+I_{01}\sin\varphi_1=I_3-I_1 , \\
&\left[\frac{\Phi_0}{2\pi R_n}\right]\frac{d\varphi_2}{dt}+I_{02}\sin\varphi_2=I_2-I_1 , \\
&\left[\frac{\Phi_0}{2\pi R_n}\right]\frac{d\varphi_3}{dt}+I_{03}\sin\varphi_3=I_4-I_1 , \\
&\left[\frac{\Phi_0}{2\pi R_n}\right]\frac{d\varphi_4}{dt}+I_{04}\sin\varphi_4=I_4-I_2 , \\
&\left[\frac{\Phi_0}{2\pi R_n}\right]\frac{d\varphi_5}{dt}+I_{05}\sin\varphi_5=I_4-I_3 , \\
&\left[\frac{\Phi_0}{2\pi R_n}\right]\frac{d\varphi_6}{dt}+I_{06}\sin\varphi_6=I_3-I_2 ,
\end{aligned} \tag{4}$$

where I_{0i} is the maximum Josephson current of the ith junction and R_n is the resistive parameter, which is taken to be common to all the junctions. In order to obtain a system of differential equations for the superconducting phases, we need to express the currents on the right-hand side of Eqs. (4) in terms of the fluxes. This is done by inverting the matrix of mutual inductance coefficients M_{ij} in Eq. (2) so that

$$I_i = \sum_{j=1}^{4} M_{ij}^{-1}(\Phi_j - \mu_0 \mathbf{H} \cdot \mathbf{S}_j), \quad i = 1,4 . \tag{5}$$

We can then make use of Eq. (3) to express the fluxes in terms of the superconducting phases and substitute the result in Eq. (5). In this way the currents are expressed completely in terms of the superconducting phases and of the forcing term $\mu_0 \mathbf{H} \cdot \mathbf{S}_i$. More explicitly, the matrix of the mutual inductance coefficients can be taken, for sym-

metry reasons, as follows: $M_{ij}=L_0$ for $i=j$, and $M_{ij}=-M_0$ for $i\neq j$. With this choice of the coefficient matrix we can easily find its inverse, so that, noticing that $\sum_{j=1}^{4}\Phi_j=0$ and that $\sum_{j=1}^{4}\mu_0\mathbf{H}\cdot\mathbf{S}_j=0$, we write

$$I_i=\frac{\Phi_i-\mu_0\mathbf{H}\cdot\mathbf{S}_i}{L_0+M_0},\quad i=1,\ldots,4\ . \tag{6}$$

We may notice that, for symmetry reasons, $L_0=3M_0$. Making use now of Eqs. (3), and defining the nonlinear Josephson operator L_{Jk} as follows: $L_{Jk}\varphi_k=d\varphi_k/d\tau+\beta_{0k}\sin\varphi_k$, where $\beta_{0k}=I_{0k}(L_0+M_0)/\Phi_0$, and $\tau=[2\pi R_n/(L_0+M_0)]t$, we can finally write

$$\begin{aligned}
L_{J1}\varphi_1&=N_3-N_1-\frac{1}{2\pi}(2\varphi_1+\varphi_2+\varphi_3-\varphi_5+\varphi_6)-\frac{\mu_0\mathbf{H}\cdot(\mathbf{S}_3-\mathbf{S}_1)}{\Phi_0}\ ,\\
L_{J2}\varphi_2&=N_2-N_1-\frac{1}{2\pi}(\varphi_1+2\varphi_2+\varphi_3-\varphi_4-\varphi_6)-\frac{\mu_0\mathbf{H}\cdot(\mathbf{S}_2-\mathbf{S}_1)}{\Phi_0}\ ,\\
L_{J3}\varphi_3&=N_4-N_1-\frac{1}{2\pi}(\varphi_1+\varphi_2+2\varphi_3+\varphi_4+\varphi_5)-\frac{\mu_0\mathbf{H}\cdot(\mathbf{S}_4-\mathbf{S}_1)}{\Phi_0}\ ,\\
L_{J4}\varphi_4&=N_3-N_2-\frac{1}{2\pi}(\varphi_2-\varphi_3-2\varphi_4-\varphi_5-\varphi_6)-\frac{\mu_0\mathbf{H}\cdot(\mathbf{S}_4-\mathbf{S}_2)}{\Phi_0}\ ,\\
L_{J5}\varphi_5&=N_4-N_3-\frac{1}{2\pi}(\varphi_1-\varphi_3-\varphi_4-2\varphi_5+\varphi_6)-\frac{\mu_0\mathbf{H}\cdot(\mathbf{S}_4-\mathbf{S}_3)}{\Phi_0}\ ,\\
L_{J6}\varphi_6&=N_3-N_2-\frac{1}{2\pi}(\varphi_1-\varphi_2+\varphi_4-\varphi_5+2\varphi_6)-\frac{\mu_0\mathbf{H}\cdot(\mathbf{S}_3-\mathbf{S}_2)}{\Phi_0}\ .
\end{aligned} \tag{7}$$

We thus solve this system of coupled nonlinear ordinary differential equations by a standard fourth-order Runge-Kutta algorithm in terms of the superconducting phases and make use of Eqs. (3) and (5) to derive the flux and current distribution in the tetrahedral network.

III. STATIONARY MAGNETIC STATES

We studied the stationary magnetic states of the tetrahedral system for two field orientations, one parallel and one perpendicular to the tetrahedron base plane. For each field orientation we took the β_{0i} coefficients, which represent the effective coupling among the junctions, to be identical for all the JJ's in one case, and uniformly distributed about a mean value β_0 in the case of inhomogeneities in the junction parameters. In order to carry out the scalar product between the applied field $\mathbf{H}$ and the area vectors $\mathbf{S}_i$ in Eqs. (7), we used an orthogonal system of axes, identifying the x-y plane with the tetrahedron base plane. Numerical results were obtained by starting from ZFC conditions (null phases at zero applied field) and by giving small enough increments $\Delta\mathbf{H}$ to the field value, after having completely determined the stationary magnetic state for the previous $\mathbf{H}$ value. For this purpose, we carried out the time integration process for a long enough time interval to allow the system to reach equilibrium before starting a new integration process. After having forced the system to a maximum value of the modulus of the external field $H_{\max}$, we gradually turned the external forcing term off and observed the remanent flux Φ_{REM} in the system.

Let us then start by illustrating the results obtained for field orientations along the z axis under the assumption that all JJ's are identical. In Figs. 2(a) and 2(b) we show

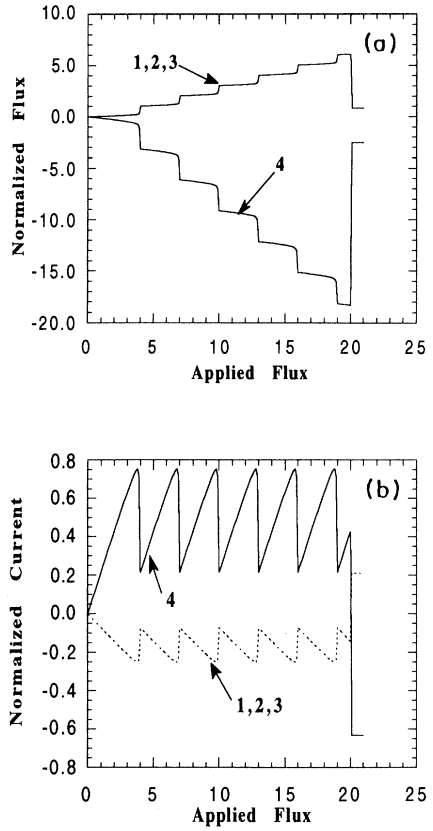

FIG. 2. Flux (a) and current (b) distribution in the tetrahedral network of Josephson junctions and inductances of Fig. 1(b) as a function of the applied flux Φ_{ex}/Φ_0. All the junctions are taken as identical. The fluxes Φ_1, Φ_2, and Φ_3 (1,2,3) and Φ_4 (4) are normalized to the flux quantum Φ_0, while the currents I_1, I_2, and I_3 (1,2,3) and I_4 (4) are divided by the maximum Josephson current I_0 of the junctions. In this run the applied magnetic field is orthogonal to the base plane and the parameter values are the following: $\beta_0=4$, $\Phi_{ex}^{MAX}=20\Phi_0$.

the applied flux dependence of the fluxes Φ_k ($k=1,\ldots,4$) and of the currents I_k ($k=1,\ldots,4$) for the following choice of parameters: $\beta_0=4$, $\Phi_{ex}^{MAX}=\mu_0 H_{max} S_0=20\Phi_0$; in Figs. 3(a) and 3(b), on the other hand, the flux and current distribution in the system is calculated for the following parameter values: $\beta_0=6$, $\Phi_{ex}^{MAX}=20\Phi_0$. From Figs. 2 and 3 we may notice that, as one expects from symmetry reasons, the flux and currents pertaining to faces 1, 2, and 3 are identical. The current I_4, on the other hand, circulates in such a way to produce a flux Φ_4 which opposes the applied flux Φ_{ex}. We notice a first reversible region in the flux and current distribution diagrams up to a lower threshold field H_{gc1}, whose value depends only on β_0, as it can be argued from Eqs. (7). Indeed, any flux transition in the system takes origin from a well-known mechanism appearing in superconducting loops interrupted by JJ's.[10] This mechanism can be briefly described as follows: When the total current circulating in the junctions reaches the maximum Josephson current value, a phase slip process occurs, so that the time derivative of the flux linked to the loop in which the junctions reside takes on nonzero values allowing irreversible flux penetration. Following this picture, analytic expressions for H_{gc1} will be derived in the following section. Here we only notice that H_{gc1} increases for increasing β_0 values, as it appears from Figs. 2 and 3.

For applied flux values immediately greater than $\Phi_{ex}^{(1)}=\mu_0 H_{gc1} S_0$, three flux quanta penetrate the system through each of the base junctions. In general, we may notice that, for each negative discontinuity of Φ_4 of about three flux quanta, there corresponds a similar discontinuity of about Φ_0 in Φ_1, Φ_2, and Φ_3. This means that the three flux quanta entering face 4 must exit the system through faces 1, 2, and 3. At higher applied flux values the same penetration process repeats with a periodicity $\Delta\Phi_{ex}^{perp}$. Finally, when the applied field is turned off grad-

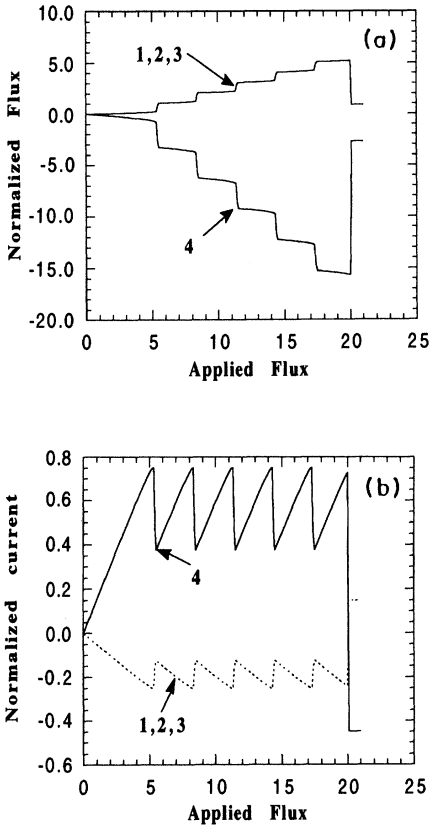

FIG. 3. Flux (a) and current (b) distribution in the tetrahedral network of Josephson junctions and inductances of Fig. 1(b) as a function of the applied flux Φ_{ex}/Φ_0. All the junctions are taken as identical. The fluxes Φ_1, Φ_2, and Φ_3 (1,2,3) and the flux Φ_4 (4) are normalized to Φ_0, while the currents I_1, I_2, and I_3 (1,2,3) and the current I_4 (4) are divided by the maximum Josephson current I_0 of the junctions. In this run the applied magnetic field is orthogonal to the base plane and the parameter values are the following: $\beta_0=6$, $\Phi_{ex}^{MAX}=20\Phi_0$.

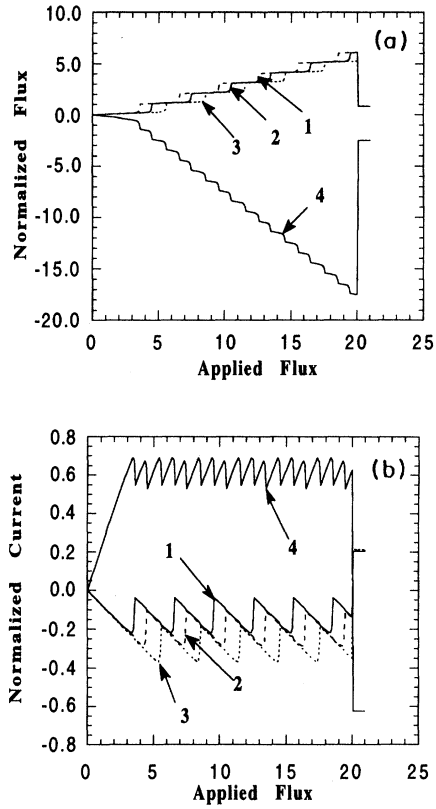

FIG. 4. Flux (a) and current (b) distribution in the tetrahedral network of Josephson junctions and inductances of Fig. 1(b) as a function of the applied flux Φ_{ex}/Φ_0. The maximum Josephson currents of the junctions are taken to vary about a mean value I_0. The fluxes Φ_1 (1), Φ_2 (2), Φ_3 (3), and Φ_4 (4) are normalized to Φ_0, while the currents I_1 (1), I_2 (2), I_3 (3),and I_4 (4) are divided by the average maximum Josephson current I_0 of the junctions. In this run the applied magnetic field is orthogonal to the base plane and $\Phi_{ex}^{MAX}=20\Phi_0$. The ratios β_{0k}/β_0 are taken, in increasing order of k values, as follows: 1.10, 1.15, 0.95, 0.90, 1.05, 0.85, with $\beta_0=4$.

ually the remanent flux Φ_{REM} for $\beta_0=4$ and $\beta_0=6$ is of about $3\Phi_0$.

The inhomogeneities in the maximum Josephson currents, and thus in β_0, break the symmetric behavior of the system as described above. Indeed, as one can notice from Figs. 4(a) and 4(b), flux transitions now occur in a more specific way. Having taken the ratios β_{0k}/β_0, in increasing order of the k values, as follows: 1.10, 1.15, 0.95, 0.90, 1.05, and 0.85, junction JJ4 results in the weakest junction in the base loop, and JJ5 the strongest. Among the remaining junctions, JJ6 is the weakest, and JJ2 the strongest. We then see that the first flux transition occurs because of a 2π phase slip in JJ4. When the flux quantum must decide which face to exit from, it always chooses the one in which the same junction is located (face 2, in this case). Next, the second flux quantum penetrates through JJ3, existing from face 1. Finally, the third flux transitions occurs because the current in JJ5 reaches its maximum value. This penetration mechanism repeats for increasing field values. We can finally notice that, since the relative strength of JJ4 is 0.90, the lower threshold field value, which can be estimated by closely looking at Figs. 4(a) and 4(b), is depressed with respect to the corresponding value obtainable from Figs. 2(a) and 2(b) for the symmetric case and for the same values of the parameters.

When we apply the external field in a direction parallel to the tetrahedron base plane and, as a particular choice, at a right angle to one of the sides of the base, we obtain the numerical results shown in Figs. 5–7 for the same variables and for the same choices of parameters as in Figs. 2 and 3. In particular, in Figs. 5(a) and 5(b) we show the flux and current external field dependence in the case of homogeneous junction coupling for $\beta_0=4$. Again,

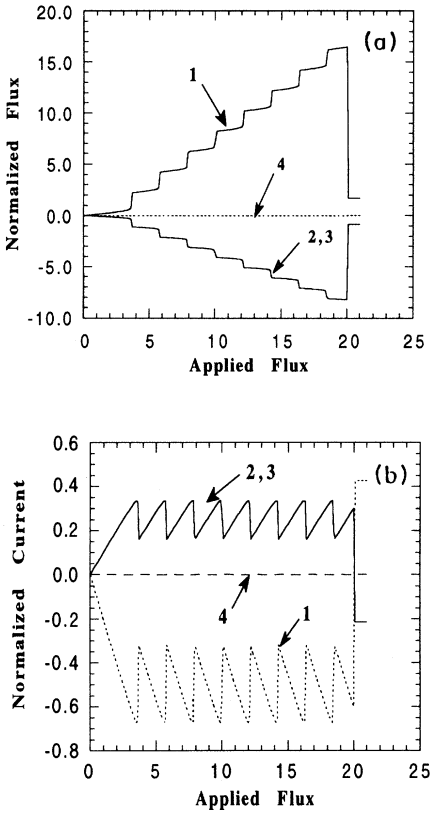

FIG. 5. Flux (a) and current (b) distribution in the tetrahedral network of Josephson junctions and inductances of Fig. 1(b) as a function of the applied flux Φ_{ex}/Φ_0. All the junctions are taken as identical. The fluxes Φ_1 (1), Φ_2, and Φ_3 (2,3), and the flux Φ_4 (4) are normalized to Φ_0, while the currents I_1 (1), I_2, and I_3 (2,3), and the current I_4 (4) are divided by the maximum Josephson current I_0 of the junctions. In this run the applied magnetic field is parallel to the base plane and orthogonal to one of the base sides. The parameter values are as in Fig. 2.

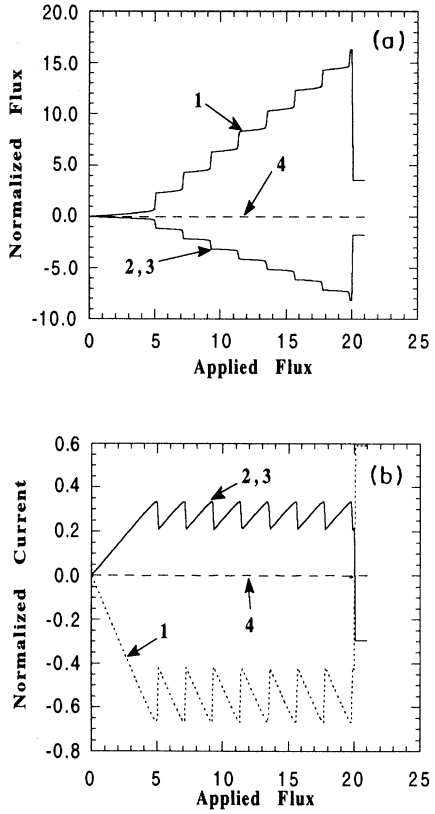

FIG. 6. Flux (a) and current (b) distribution in the tetrahedral network of Josephson junctions and inductances of Fig. 1(b) as a function of the applied flux Φ_{ex}/Φ_0. All the junctions are taken as identical. The fluxes Φ_1 (1), Φ_2 and Φ_3 (2,3), and the flux Φ_4 (4) are normalized to Φ_0, while the currents I_1 (1), I_2 and I_3 (2,3), and the current I_4 (4) are divided by the maximum Josephson current I_0 of the junctions. In this run the applied magnetic field is parallel to the base plane and orthogonal to one of the base sides. The parameter values are as in Fig. 3.

for symmetry reasons, we have $\Phi_4=0$, $\Phi_2=\Phi_3$, and $\Phi_1=-2\Phi_2$. We notice that the first irreversible flux penetration in this case occurs at a lower external flux value when compared to the corresponding case of Fig. 2, and that the flux discontinuities are of about two flux quanta for Φ_1. In addition, the flux transition periodicity $\Delta\Phi_{ex}^{para}$ is lower than in the previous case. The same characteristics are also present in Figs. 6(a) and 6(b), where we show the flux and current distributions for $\beta_0=6$. Finally, when the applied field is turned off gradually, we notice that $\Phi_{REM}\approx 2\Phi_0$ for $\beta_0=4$, while $\Phi_{REM}\approx 4\Phi_0$ for $\beta_0=6$.

The effect of inhomogeneities in β_0 can be detected by looking at Figs. 7(a) and 7(b), where the external flux dependence of the fluxes and currents is shown for the same values of the ratios β_{0k}/β_0 as before. In this case, flux transitions occur in the following order. First, one flux quantum penetrates face 3 through JJ1 and exits from face 1. Successively, a second flux quantum penetrates face 2 through JJ2 and exits from face 1. The same penetration mechanism is reported for higher applied flux values. Naturally, the same type of reasoning as above applies in this case when one tries to justify this particular penetration process. In this case, however, the junctions responsible for flux penetration (JJ1 and JJ2) have both relative strength greater than 1. Therefore, the lower threshold field value is expected to be greater than the corresponding one in the symmetric case. One can indeed notice this feature by closely comparing the field value at which the first discontinuity appears in Figs. 4(a) and 4(b) and Figs. 7(a) and 7(b). This is a very particular case, though. In fact, had we chosen a different field direction for the particular distribution of the β_{0k}/β_0 ratios given above, a reduction of the lower threshold field value would be expected.

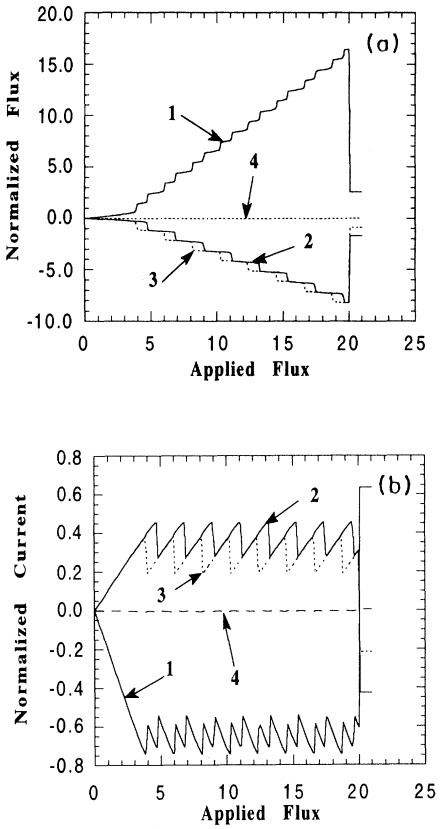

FIG. 7. Flux (a) and current (b) distribution in the tetrahedral network of the Josephson junctions and inductances of Fig. 1(b) as a function of the applied flux Φ_{ex}/Φ_0. The maximum Josephson currents of the junctions are taken to vary about a mean value I_0. The fluxes Φ_1 (1), Φ_2 (2), Φ_3 (3), and Φ_4 (4) are normalized to Φ_0, while the currents I_1 (1), I_2 (2), I_3 (3), and I_4 (4) are divided by the average maximum Josephson current I_0 of the junctions. In this run the applied magnetic field is parallel to the base plane and orthogonal to one of the base sides and $\Phi_{ex}^{MAX}=20\Phi_0$. The ratios β_{0k}/β_0 are taken, in increasing order of k values, as follows: 1.10, 1.15, 0.95, 0.90, 1.05, 0.85, with $\beta_0=4$.

IV. LOWER THRESHOLD FIELD

As we have already noticed in the preceding section, for each of the Φ_k vs Φ_{ex} graphs shown above, a lower threshold field H_{gc1}, which separates a first reversible magnetic regime from an irreversible one, is present. We shall now analyze in which cases this field does exist, and, if it exists, what its value is. We shall consider the homogeneous β_0 parameter case only, for simplicity.

Let us start by considering the external field applied in the direction perpendicular to the base of the tetrahedral network. For symmetry reasons we can distinguish two groups of junctions, the first consisting of the junctions lying on the base (JJ3, JJ4, JJ5), each having phase difference φ_b, the second consisting of the remaining three junctions JJ1, JJ2, JJ6, whose phase difference is taken to be φ_a. The stationary equations for the phases φ_a and φ_b are obtained from Eqs. (7), and can be summarized as follows:

$$I_0\sin\varphi_a=0, \quad I_0\sin\varphi_b=I_b-I_a \ , \tag{8}$$

where I_a and I_b are the currents circulating in the side faces and in the base face, respectively. By making use of fluxoid quantization [Eqs. (3)] and of the current-flux relations [Eqs. (6)] under ZFC conditions, and by setting $\Phi_a=\Phi_1=\Phi_2=\Phi_3$, and $\Phi_b=\Phi_4$, we may write

$$\beta_0\sin\left[\frac{2\pi\Phi_a}{\Phi_0}\right]+4\frac{\Phi_a}{\Phi_0}=\frac{4}{3}\frac{\Phi_{ex}}{\Phi_0}, \quad \Phi_b=-3\Phi_a \ . \tag{9}$$

The first of the above equations is similar to the stationary equation for a superconducting quantum interference device (SQUID).[10] Following the same type of reasoning as for this well-known system, one finds that the Φ_a vs Φ_{ex} curve does not present discontinuities only for $\beta_0<2/\pi$, while irreversible flux transitions are present for $\beta_0\geq 2/\pi$. This gives the existence condition for a lower threshold field in the tetrahedral network when **H** is applied perpendicularly to the base plane of the system. As far as the lower threshold field value is concerned, we

can still make use of the SQUID analysis,[10] so that, by Eqs. (9) one finds

$$H_{gc1}=\frac{3}{4}\frac{\beta_0\Phi_0}{\mu_0 S_0}\left\{\left[1-\left[\frac{2}{\pi\beta_0}\right]^2\right]^{1/2}+\left[\frac{2}{\pi\beta_0}\right]\sin^{-1}\left[1-\left[\frac{2}{\pi\beta_0}\right]^2\right]^{1/2}\right\}. \tag{10}$$

Flux transitions at higher fields are found to occur for the following field values $\Phi_{ex}^{(k)}$:

$$\Phi_{ex}^{(k)}=\Phi_{ex}^{(1)}+3(k-1)\Phi_0, \quad k=2,3,\ldots . \tag{11}$$

We now turn to **H** parallel to the base plane as shown in Fig. 1(b). In this case we may set $\Phi_2=\Phi_3$, $\Phi_1=-2\Phi_2$, and $\Phi_4=0$. The stationary equations for the phases are again obtained from Eqs. (7), and can be written as follows:

$$\begin{aligned}&\beta_0\sin\varphi_1=\frac{3\Phi_2+\sqrt{2}\Phi_{ex}}{\Phi_0}, \quad \varphi_2=\varphi_1 ,\\ &\beta_0\sin\varphi_3=2\frac{\Phi_2+(\sqrt{2}/3)\Phi_{ex}}{\Phi_0} ,\\ &\beta_0\sin\varphi_4=-\frac{\Phi_2+(\sqrt{2}/3)\Phi_{ex}}{\Phi_0}=-\frac{\beta_0\sin\varphi_1}{3} ,\\ &\varphi_5=\varphi_4 \text{ and } \varphi_6=0 .\end{aligned} \tag{12}$$

Fluxoid quantization under ZFC conditions gives $2\pi\Phi_2=(\varphi_4-\varphi_1)\Phi_0$. Adding this constraint to Eqs. (12), we can write

$$\begin{aligned}&\beta_0\sin\varphi_1=\frac{3\Phi_2+\sqrt{2}\Phi_{ex}}{\Phi_0}, \quad \sin\varphi_4=-\frac{\sin\varphi_1}{3} ,\\ &\varphi_4-\varphi_1=2\pi\frac{\Phi_2}{\Phi_0} .\end{aligned} \tag{13}$$

An exact solution to Eqs. (13) can be found, but here we prefer to exhibit an approximated analytic expression. Applying a standard procedure, we express all the quantities in Eqs. (13) in terms of φ_1 and get, making use of the first equation, a Φ_{ex} vs φ_1 expression. We proceed in this way because the 2π phase slip occurs in the first and second junctions. Now, if the φ_1 vs Φ_{ex} graph does not present any discontinuity, the derivative of its inverse never goes to zero. However, if discontinuities are present, this derivative must go to zero for some values of φ_1. The phase value at which the first 2π phase slip occurs will be denoted by φ_1^*. We therefore find the following equation for φ_1^*:

$$\beta_0\cos\varphi_1^*+\frac{3}{2\pi}\left[\frac{\cos\varphi_1^*}{\sqrt{9-\sin^2\varphi_1^*}}+1\right]=0 . \tag{14}$$

If we neglect $\sin\varphi_1^*$ under the square root sign in Eq. (14), we immediately find

$$\varphi_1^*=\cos^{-1}\left[-\frac{3}{1+2\pi\beta_0}\right] . \tag{15}$$

Equation (15) determines the following existence condition for H_{gc1}: $\beta_0\geq 1/\pi$. The lower threshold field value is therefore obtained by substituting this value of φ_1^* in the Φ_{ex} vs φ_1 expression, so that

$$H_{gc1}=\frac{\beta_0\Phi_0}{\sqrt{2}\mu_0 S_0}\left\{\sqrt{1-[3/(1+2\pi\beta_0)]^2}+\frac{3}{2\pi\beta_0}\left[\cos^{-1}\left[-\frac{3}{1+2\pi\beta_0}\right]+\sin^{-1}\left(\tfrac{1}{3}\sqrt{1-[3/(1+2\pi\beta_0)]^2}\right)\right]\right\} . \tag{16}$$

Successive flux transitions are found by adding the quantity $2k\pi$ (k being an integer) to the solution for φ_1^*. Therefore, we find

$$\Phi_{ex}^{(k)}=\Phi_{ex}^{(1)}+\frac{3}{\sqrt{2}}(k-1)\Phi_0, \quad k=2,3,\ldots . \tag{17}$$

The above expression confirms what has been found numerically, namely, that the flux transition periodicity $\Delta\Phi_{ex}^{perp}$ in the case when the external field is applied perpendicularly to the base plane is greater than the corresponding quantity when the external field is parallel to the tetrahedral base as in Fig. 1(b). Indeed, following Eqs. (11) and (17), we see that $\Delta\Phi_{ex}^{perp}=3\Phi_0$ and $\Delta\Phi_{ex}^{para}=(3/\sqrt{2})\Phi_0$. The numerical results obtained in the preceding section also confirm the analytic expression for the lower threshold field H_{gc1} given by Eqs. (10) and (16) for the two field orientations considered in the present work.

V. CONCLUSIONS

We studied the stationary magnetic states of the simplest 3D Josephson-junction network: a tetrahedron containing a junction on each side. The Josephson junctions were taken to be inductively coupled in order to account for the magnetic energy of the circulating currents in the system. We derived the dynamic equations for flux transition for arbitrary applied field directions in space. In particular, we analyzed two cases: in the first case, the externally applied magnetic field **H** was taken to point in the direction orthogonal to the tetrahedron base plane; in the second case, **H** was taken to be a vector lying in a

plane parallel to the tetrahedron base plane and perpendicular to one side of the tetrahedron base itself. For these two cases we determined the flux and current distributions as a function of the applied field and the lower threshold field H_{gc1} for irreversible flux penetration in terms of the effective coupling parameter β_0.

In the study of the low-field magnetic response of high-T_c granular superconductors, this simple model can be considered as a first step toward a more complex analysis, performed on a system consisting of a much higher number of grains in the same arrangement. In order to make predictions on the behavior of these larger clusters we can adopt the results obtained for 2D circuital models.[7] In these models, for large β values the penetration process of a single flux quantum in an intergranular loop determines only a local change in the current distribution; i.e., the perturbation due to the presence of an additional flux quantum in the system is limited to the region occupied by the loop itself. Under this condition the intergranular sites can be seen as almost independent entities. On the other hand, for low values of the β parameter a long-range interaction among loops exists. Applying this reasoning to 3D systems, we can argue that for large β values the results obtained for a single unit cell can be extended to larger clusters of grains, while the same is not true if β is lower than a certain crossover value. In the latter case, a complete analysis on larger systems becomes necessary. Finally, when analyzing the magnetic properties of more realistic systems, one may notice that the dimensions, the geometrical shapes, and the relative diamagnetic factors pertaining to single grains are not significant quantities for the corresponding model. Indeed, these properties play a role only in determining the effective surface of a single face of an irregular tetrahedron. In this way, one can take account of these factors by simply changing the effective values of the β parameters. As a consequence, the qualitative behavior of the dynamics of the model will be left unchanged.

[1]J. R. Clem, Physica C **153-155**, 50 (1988).
[2]D. Stroud and C. Ebner, Physica C **153-155**, 63 (1988).
[3]A. Majhofer, T. Wolf, and W. Dieterich, Phys. Rev. B **44**, 9634 (1991).
[4]R. De Luca, S. Pace, and G. Raiconi, Phys. Lett. A **172**, 391 (1993).
[5]S. Pace and R. De Luca, Physica C **180**, 176 (1991).
[6]T. Wolf and A. Majhofer, Phys. Rev. B **47**, 5383 (1993).
[7]C. Auletta, R. De Luca, S. Pace, and G. Raiconi, Phys. Rev. B **47**, 14 326 (1993).
[8]S. L. Ginzburg, V. P. Khavronin, G. Yu. Logvinova, I. D. Luzyanin, J. Hermann, B. Lippold, H. Borner, and H. Schmiedel, Physica C **174**, 109 (1991).
[9]R. De Luca, Phys. Lett. A **175**, 353 (1993).
[10]A. Barone and G. Paternò, *Physics and Applications of the Josephson Effect* (Wiley, New York, 1982).
[11]R. L. Peterson and J. W. Ekin, Phys. Rev. B **42**, 8014 (1990).
[12]G. Costabile, R. De Luca, S. Pace, A. Saggese, and A. M. Testa, IEEE Trans. Appl. Supercond. (to be published).
[13]G. Filatrella, S. Pace, G. Rotoli, and A. Saggese, Phys. Lett. A **193**, 491 (1994).
[14]S. P. Yukon and N. C. H. Lin, IEEE Trans. Appl. Supercond. (to be published).